

Simultaneous Single-Pulse Observations of Radio Pulsars: V. On the Broadband Nature of The Pulse Nulling Phenomenon in PSR B1133+16

N. D. R. Bhat¹, Y. Gupta², M. Kramer³, A. Karastergiou⁴, A. G. Lyne³, and S. Johnston⁵

¹ Centre for Astrophysics and Supercomputing, Swinburne University of Technology, Hawthorn, Vic 3122, Australia

² National Centre for Radio Astrophysics, Tata Institute of Fundamental Research, Ganeshkhind, Pune 411007, India

³ Jodrell Bank Observatory, University of Manchester, Macclesfield, Cheshire, SK11 9DL, UK

⁴ IRAM, 300 rue de la Piscine, Domaine Universitaire 38406 Saint Martin d'Hères, France

⁵ Australia Telescope National Facility, CSIRO, PO Box 76, Epping, NSW 1710, Australia

Accepted 19 October 2006

ABSTRACT

Aims. In this paper we revisit the well-known phenomenon of pulse nulling using high-quality single-pulse data of PSR B1133+16 from simultaneous multifrequency observations.

Methods. Observations were made at 325, 610, 1400 and 4850 MHz as part of a joint program between the European Pulsar Network (EPN) and the Giant Metrewave Radio Telescope (GMRT). The pulse energy time series are analysed to derive improved statistics of nulling pulses as well as to investigate the frequency dependence of the phenomenon.

Results. The pulsar is observed to be in null state for approximately 15% of the time; however, we find that nulling does not always occur simultaneously at all four frequencies of observation. We characterise the statistics of such “selective nulling” as a function of frequency, separation in frequency, and combination of frequencies. The most remarkable case of such selective nulling seen in our data is a significantly large number of nulls ($\approx 6\%$) at lower frequencies, that are marked by the presence of a fairly narrow emission feature at the highest frequency of 4850 MHz. We refer to these as “low frequency (LF) nulls.” We characterise the properties of high frequency (HF) emission at the occurrence of LF nulls, and compare and contrast them with that of “normal emission” at 4850 MHz. Our analysis shows that this high frequency emission tends to occur preferentially over a narrow range in longitude and with pulse widths typically of the order of a few milliseconds. We discuss the implications of our results for the pulsar emission mechanism in general and for the broadbandness of nulling phenomenon in particular. Our results signify the presence of an additional process of emission which does not turn off when the pulsar nulls at low frequencies, and becomes more prominent at higher frequencies. Our analysis also hints at a possible outer gap origin for this new population of pulses, and thus a likely connection to some high-energy emission processes that occur in the outer parts of the pulsar magnetosphere.

Key words. pulsars: general – pulsars: individual, PSR B1133+16 – ISM: general – radiation mechanism: non-thermal

1. Introduction

Radio emission from pulsars is known to vary on a wide range of time scales, from as short as one pulse period to many hours or days. Many pulsars are known to exhibit the phenomenon of “nulling,” where the emission appears to cease, or is greatly diminished, for a certain number of pulse periods. Typical time scales of nulling are of the order of a few pulse periods, however it may last for up to many hours in certain pulsars; for example, PSR B0826–34 which is active for only $\sim 20\%$ of the time (Durdin et al. 1979).

Ever since its discovery (Backer 1970) and early investigations (Ritchings 1976), the phenomenon of nulling has remained as a vital clue for understanding the elusive pulsar emission mechanism. Several authors have investigated this phenomenon in detail (e.g., Biggs (1992); Rankin (1986)), and it is fairly well established that (i) the phenomenon is intrinsic to the pulsar, (ii) it is possibly broadband, and (iii) the null fraction (NF) is strongly correlated to the pulse period (Biggs 1992; Ritchings 1976). It is also known that the null fraction (NF) depends on the pulsar class, and that single-core pulsars have rather low values

of NF (Rankin 1986). However, the suggested correlation between the null fraction and age is not strongly supported within a given pulsar class. As is the case with several other phenomena of pulsar signals, a satisfactory explanation for nulling, particularly the physics that governs it, remains largely elusive.

Studies of individual pulses from simultaneous multifrequency observations provide valuable insights into the pulsar emission mechanism. In particular, such studies help address the broadband nature and frequency dependence of the intrinsic phenomena such as drifting and nulling. Such studies however require coordinated multi-station observations which are hard to realise in practice. Consequently, few such studies have been reported in the past, and most of these were made in the early days of pulsar research (Backer & Fisher 1974; Davies et al. 1984; Robinson et al. 1968). Moreover, most of these experiments involved observations at only 2 to 3 frequencies, and focussed primarily on lower frequencies ($\lesssim 2.6$ GHz). These observations led to a general understanding that phenomena such as drifting, nulling and moding are generally of broadband nature at low observing frequencies.

This work is fifth in a series of papers describing simultaneous multifrequency observations of radio pulsars. Observations

were made in January 2000 as part of a joint collaborative effort between the European Pulsar Network (EPN; Lorimer et al. (1998)) and the Giant Metrewave Radio Telescope (GMRT) in India. These observations led to long stretches of high quality data for five pulsars over a wide frequency range, from 0.24 to 4.85 GHz (Bhat et al. 2001). Data at 1.4 and 4.85 GHz (from the Lovell and Effelsberg telescopes respectively) were recorded in full polarisation, while data at lower frequencies (from the GMRT) were recorded in total power. The science goals included investigation of a variety of phenomena related to pulsar emission. The earlier papers in this series focussed on polarisation and spectra of individual pulses (Karastergiou et al. (2001, 2002, 2003); Kramer et al. (2003); hereafter Paper IV). In this paper we present an in-depth analysis of the pulse nulling phenomenon using data at 4 frequencies for PSR B1133+16, with particular emphasis on investigating the broadband nature of the phenomenon.

The remainder of the paper is organised as follows. In §2 we describe the details of observations and data reduction. Pulse energy time series are presented in §3, and we discuss the statistics of nulling in §4. In later sections we focus our attention on some key results from our analysis, most notable of which is evidence for a “selective nulling” phenomenon that is characterised by mostly single-peaked, narrow emission features at the highest frequency, 4850 MHz, and nulls at lower frequencies. Our conclusions are presented in §7.

2. Simultaneous Multifrequency Observations

The data presented in this paper was obtained from simultaneous observations at four different frequencies, viz. 325, 610, 1400 and 4850 MHz. Data at the higher two frequencies were recorded over bandwidths of 500 MHz (Effelsberg) and 32 MHz (Lovell), while the data-taking system at the GMRT employed a bandwidth of 16 MHz. The observations using Effelsberg and Lovell have been described by Karastergiou et al. (2002). Observations at the GMRT capitalised on the instrument’s unique capability whereby observations at more than one frequency can be done simultaneously, by configuring the telescope in a multiple sub-array mode (Gupta, Gothoskar, & Bhat 2002). In this mode, data at the two frequencies were recorded by the same data logging system, where the signals from both the frequencies were added together after square-law detection, and the pulsar dispersion delay was used to separate the two data streams in the off-line analysis. Data from all telescopes were stored for off-line processing.

At Effelsberg and Lovell, data were recorded as a single, uninterrupted session, whereas data-taking at the GMRT was split into two sessions (of durations 1932 and 2441 pulse periods, i.e., in total 4373 pulse periods) due to maximum file size limitations for a single scan. For the convenience of analysis, as well as to allow useful cross-checks of any statistical analyses that we perform, we treat data from the two sessions as two separate data sets, and hereafter refer to them as data set I and data set II, respectively. Data from all three telescopes were converted to a common EPN format and time-aligned following the procedures detailed in Karastergiou et al. (2001). Further, data for all four frequencies were smoothed to an effective time resolution of $1159.8 \mu\text{s}$ (off-line dispersion was performed on data from the GMRT, while data at Lovell were recorded after correcting for dispersion on-line)¹. A small fraction of the data (roughly 9%), particularly at the GMRT frequencies, was affected by ra-

dio frequency interference (RFI), and is hence excluded from subsequent analyses.

As described in Paper IV, flux density calibration was performed at all four frequencies. At Effelsberg and Lovell, the pulsar data was compared to that of a pre-calibrated noise diode, which itself was compared to the strength of known flux calibrators observed during pointing observations before, after and during the observations. The estimated uncertainty resulting from this calibration scheme is about 10%. At the GMRT, known flux calibrators such as 3C147, 3C295 and 3C286 were observed before and after every pulsar observation. Unlike the pulsar data, the calibration data were gathered separately at two frequencies, i.e., one frequency at a time, using the summed signal from only those antennas that were selected for the frequency. From these data, an effective calibration scale was computed for each of the two frequencies. Using the nearest available calibration source, this scale was then applied to the “on-off” deflection of the pulsar, separately for each frequency of observation, in order to flux calibrate the pulsar signal at both frequencies. As demonstrated in Paper IV, the average flux densities estimated from our calibration scheme are consistent with what is known from literature at the frequencies of observation.

3. Pulse Energy Time Series

3.1. Detection of null and on states

Conventionally, a null state signifies our inability to detect pulsar emission over one or more pulse periods. This *inability* depends on the sensitivity of the observing system, and consequently, sensitive single-pulse observations are ideal for accurate characterisation of pulsar nulling properties. For PSR B1133+16, typical flux densities at our observing frequencies are ~ 20 to ~ 100 times larger than the minimum detectable flux densities obtained from our observing parameters. Such high quality data allow an in-depth study of the nulling behaviour of this pulsar.

Traditionally, the occurrence of nulling in a pulsar is characterised by the pulse nulling statistics that are derived from pulse energy distributions (e.g. Biggs 1992; Ritchings 1976). ON and OFF pulse energy histograms for our four frequency observations are shown in Fig. 1. At lower frequencies, we can see a classical separation of the ON pulse histograms into two components, with a zero energy excess that signifies the presence of nulling. At the higher two frequencies, the distributions tend to merge with each other, as the signal-to-noise ratio (S/N) for the pulses is, on the whole, poorer.

Using these distributions and a method similar to that described by Ritchings (1976), we have estimated the null fraction (NF) values for the two data sets (Table 1), at the two lower frequencies. The method does not yield meaningful estimates at the higher frequencies 1400 and 4850 MHz, where the ON and OFF distributions tend to merge. The lower and upper limits obtained in this manner are denoted as α_{low} and α_{high} respectively. Values for the NF at a given frequency are quite consistent between the two data sets. Furthermore, they are consistent with values reported (at 408 MHz) in the literature for this pulsar (Biggs 1992; Ritchings 1976).

Whereas pulse energy distributions provide a good tool for estimating statistical values related to the nulling phenomenon, we need a different approach to identify individual null pulses at each frequency of observation. We do this by comparing the ON pulse energy estimate with a threshold based on the system noise level. The uncertainty in the pulse energy estimate $\sigma_{ep,on}$ is given by $\sqrt{n_{on}} \sigma_{off}$, where n_{on} is the number of ON pulse bins and

¹ The dispersion effect is negligible at the highest frequency 4850 MHz, and hence no correction was applied for data from Effelsberg.

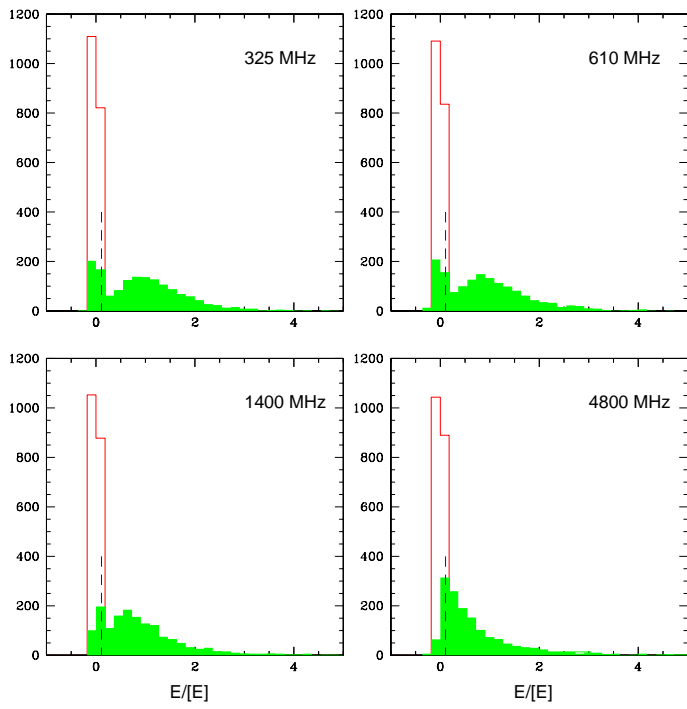


Fig. 1. ON and OFF pulse energy histograms (shown as shaded and unshaded regions respectively) for the data set I at four frequencies of observation, 325, 610, 1400 and 4850 MHz. The pulse energy E is normalised with its running mean over 200 pulse periods, $[E]$. The vertical dashed line is the mean of $3\text{-}\sigma$ pulse energy thresholds that are used to define the state of the pulse.

Table 1. Estimates of the null fraction at 325 and 610 MHz[†]

Frequency (MHz)	Data set I		Data set II	
	α_{low}	α_{high}	α_{low}	α_{high}
325	15%	22.5%	15.5%	24.5%
610	12.5%	23%	14.5%	24%

[†] Not obtainable at 1400 and 4850 MHz (see text for justification).
Note: The null fraction at 408 MHz $\sim 15 \pm 3\%$ (Ritchings 1976).

σ_{off} is the rms of the OFF pulse region. Using this as a threshold, we define pulses with ON pulse energy smaller than $3 \times \sigma_{\text{ep,on}}$ as null pulses.

Results from this classification are illustrated in Fig. 2 which shows the time series of pulse energies (on a logarithmic scale for clarity). The blue band of filled circles denotes the $3\text{-}\sigma$ threshold. As can be seen, the single pulse energies vary by large amounts. Some of the slower time scale variations are likely due to interstellar scintillations (ISS), and this effect is discussed in detail in Appendix I. At each frequency, a significant number of individual null pulses can easily be detected.

3.2. Binary Time Series of Pulse States

From the above classification scheme for null pulses, we derive a “binary time series” of pulse states where the “on” and “off” (null) states of pulsar emission are assigned values of “1” and “0”, respectively. An example of such a time series of pulse states is shown in Fig. 3 where, for clarity, the length of the time

series is restricted to ≈ 200 pulse periods. This is enough to illustrate the general trends, and can be summarised as follows:

1. To first order, we find that the nulling phenomenon is broadband – in that most pulses are in null state simultaneously at all four frequencies – over a wide range of 0.3 to 4.9 GHz, and spanning a frequency ratio of ~ 15 , i.e., 4 octaves.
2. However, there is a significant number of pulses where nulling does *not always* occur simultaneously at all frequencies.
3. Furthermore, there appears to be a tendency for what we term as “selective nulling,” wherein the null state is restricted to two or three frequencies of observation (more often the lower frequencies), and sometimes just to a single frequency.

To study these aspects more quantitatively, we compute different statistics from the four frequency binary time series of pulse energies, and investigate their dependencies on frequency and frequency separation.

4. Statistics of Null Pulses

The simplest useful statistical quantity is the null count, which is simply the total number of pulses that are in a null state in the binary time series. This null count, when normalised by the total number of pulses in the data set, can be thought of as an estimate of the null fraction. The usefulness of our data set is that such null counts can be estimated for each frequency, as well as for different combinations of frequencies. For the latter, only pulses that null simultaneously for the desired combination of frequencies are included in the null count.

Table 2 shows a summary of these results, where numbers are tabulated separately for data sets I and II. Column (1) is a listing of the specific class (i.e., frequency or the combination of frequencies) for which the null count is computed. Columns (2) and (4) list the number of null pulses (and their percentages) for a given class.

The first thing to note about the results in this table is that our single frequency null counts are fairly consistent with our estimates of null fraction in Table 1, with the exception of the 610 MHz estimate for data set II which is biased by the effect of ISS (see Appendix A). Furthermore, the null counts generally appear to reduce systematically as one goes from the single frequency counts to those for two or more frequency combinations, suggesting that the nulling phenomenon is somewhat frequency dependent. Thus, for example, the single frequency data show a null fraction of typically $\sim 16\%$, while the estimate is approximately half this value for the combination of all observing frequencies. Furthermore, a scrutiny of the numbers in columns (2) and (4) also reveals a tendency for the null fraction to decrease with the frequency coverage of the data. This is better illustrated in Fig. 4 which shows a plot of “mean null counts” against the number of frequencies in the null class type under consideration (column 1 of Table 2). Hence, our observations strongly suggest that the nulling phenomenon is *not always* broadband. The most significant exceptions to the above trends involve data from 610 and 1400 MHz observations, especially for data set II. We believe that the large fluctuations and deep fading of pulse intensities at these frequencies, which lead to increased null counts, is due to the phenomenon of ISS. This is addressed in detail in Appendix A.

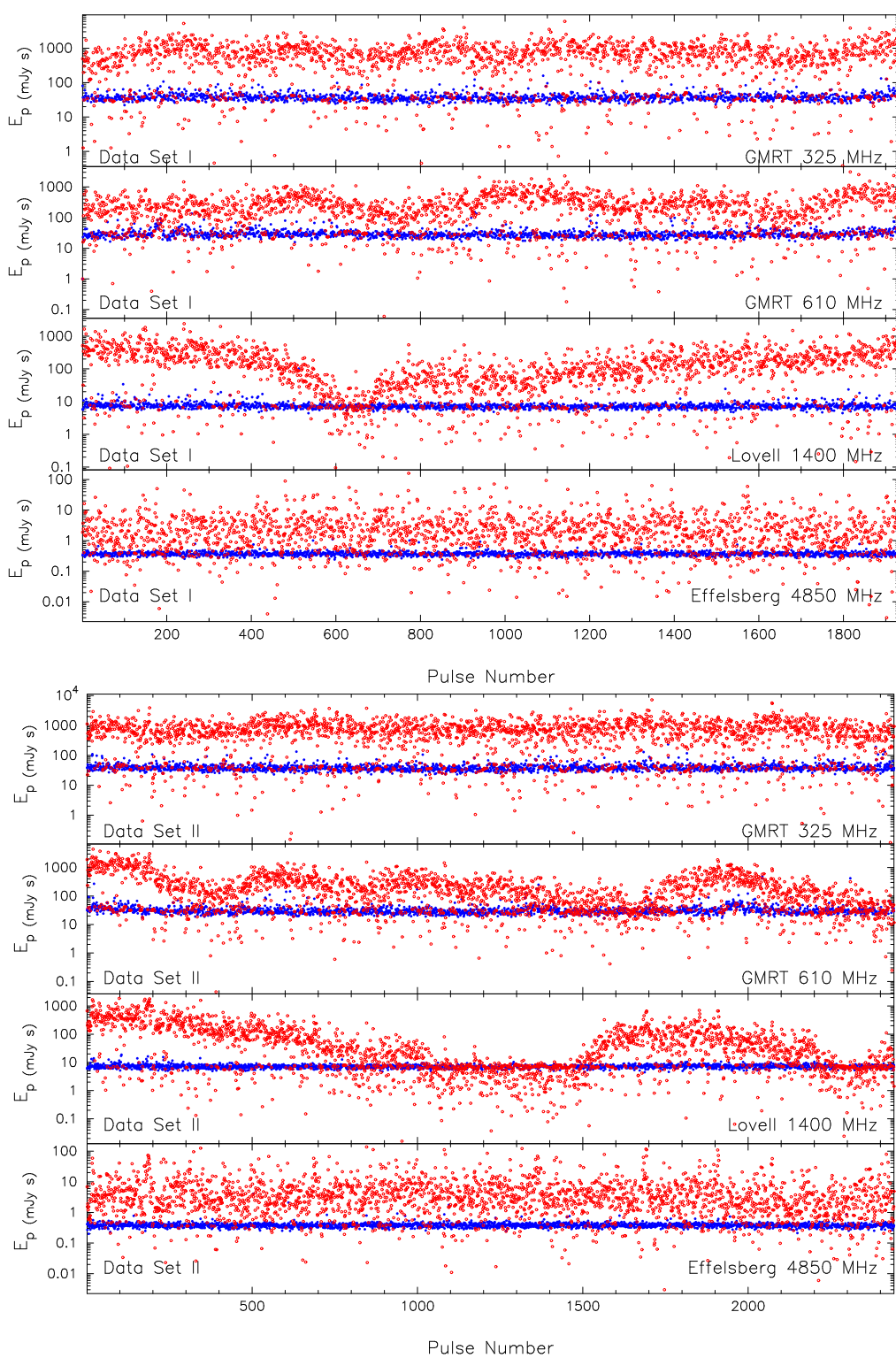


Fig. 2. Pulse energy time series of PSR B1133+16 at 325, 610, 1400 and 4850 MHz (top to bottom in each panel, with *top* panel for the data set I and *bottom* panel for the data set II). The blue band of filled circles represents the thresholds below which a pulse is considered to be in null state. For 325, 610 and 1400 MHz, energy estimates that are below zero are given a fixed value of 1 in the plots. The energy estimates are plotted on logarithmic scales for easy identification of null pulses.

4.1. Nulls and Bursts: Evidence for a Frequency Dependence?

We digress briefly to address the question of whether the null and burst durations have any frequency dependence, as this is something that has never been reported before in the literature.

Fig. 3 hints at such a possibility, with a tendency for shorter null durations at higher frequencies.

In order to quantify this, we have computed individual null and burst durations from our binary time series of pulse states and the results are summarised in Fig. 5 in the form of his-

Table 2. Summary of null counts and exclusive nulls for various frequency combinations

Null Class (1)	Data Set I (1932 pulses) ^a		Data Set II (2441 pulses) ^a	
	Null Count (2)	Exclusive Nulls (3)	Null Count (4)	Exclusive Nulls (5)
4-frequency nulls: 325+610+1400+4850	145 (8.3)		147 (6.6)	
3-frequency nulls: 325+610+1400	207 (11.8)	62 (3.5)	315 (14.2)	168 (7.6)
325+610+4850	155 (8.8)	10 (0.6)	152 (6.8)	5 (0.2)
325+1400+4850	152 (8.7)	7 (0.4)	162 (7.3)	15 (0.7)
610+1400+4850	162 (9.2)	17 (1.0)	164 (7.4)	17 (0.8)
2-frequency nulls: 325+610	264 (15.1)	47 (2.7)	354 (15.9)	34 (1.5)
325+1400	222 (12.7)	8 (0.5)	348 (15.7)	20 (0.9)
325+4850	162 (9.2)	0 (0.0)	168 (7.6)	1 (0.1)
610+1400	233 (13.3)	9 (0.5)	433 (19.5)	101 (4.5)
610+4850	189 (10.8)	17 (1.0)	177 (8.0)	8 (0.4)
1400+4850	177 (10.1)	8 (0.5)	190 (8.6)	11 (0.5)
1-frequency nulls: 325	296 (16.9)	17 (1.0)	413 (18.6)	23 (1.0)
610	334 (19.1)	27 (1.5)	590 (26.6) ^b	110 (4.9)
1400	290 (16.5)	34 (1.9)	848 (38.2) ^b	369 (16.6)
4850	279 (15.9)	75 (4.3)	222 (10.0)	18 (0.8)

Note: The numbers in parentheses are the percentage null counts, and can be considered as rough estimates of the null fraction.

^a The number of bad pulses (excluded from the analysis): 180 and 220 respectively for the data set I and the data set II (see text).

^b Estimation of the null count is probably biased by the interstellar scintillation (ISS) effects (see Appendix A for further details).

tograms of null and burst lengths. The following conclusions can be drawn from these results:

1. This pulsar shows predominantly short duration nulls (up to four pulse periods). A vast majority of the observed nulls have durations of just one pulse period, with a smaller fraction extending to durations of two or more pulse periods.
2. The number of longer duration nulls (i.e. two or more pulse periods) seems to decrease with an increase in frequency. This trend is very clear for data set I.
3. The burst duration varies over a wide range from 1 to 30 pulse periods and seems to follow a roughly exponential-type distribution. Majority of these bursts have durations of 1 to 10 pulse periods.
4. Although there does not seem to be any systematic trend for burst durations with frequency, short duration bursts are comparatively larger in number at our highest observing frequency of 4850 MHz.

To further explore the frequency dependence of null durations, we study the ratio of the number of nulls of single pulse duration, to the number of nulls of two, three and four pulse durations. Figure 6 shows these ratios for each of the four frequencies. It is clear from this that the relative number of longer duration nulls does indeed decrease significantly with increasing frequency. Thus this pulsar appears to null more often for relatively longer durations at lower frequencies.

4.2. Selective Nulling: “Exclusive Null” Pulses

In order to characterise the selective nulling phenomenon pointed out in section §3.2, we compute the number of “exclusive nulls” for every frequency combination – these are the

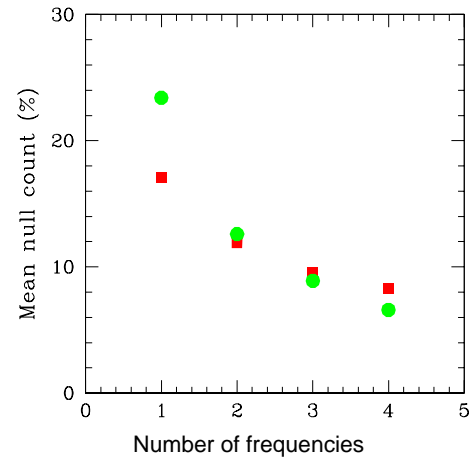


Fig. 4. Mean null counts (in percentage) are plotted against the number of observing frequencies. This quantity is essentially the mean of all null counts in a given type of null class (see column 1 of Table 2). The red (squares) and green (circles) symbols correspond to the data sets I and II respectively. The single-frequency point for the data set II is biased upward due to an apparent excess in null counts at 610 and 1400 MHz for this data set. The number of simultaneous nulls tends to decrease with the frequency coverage of the data.

counts of pulses that null *exclusively* for that frequency combination. For instance, for the 325+610+1400 MHz combina-

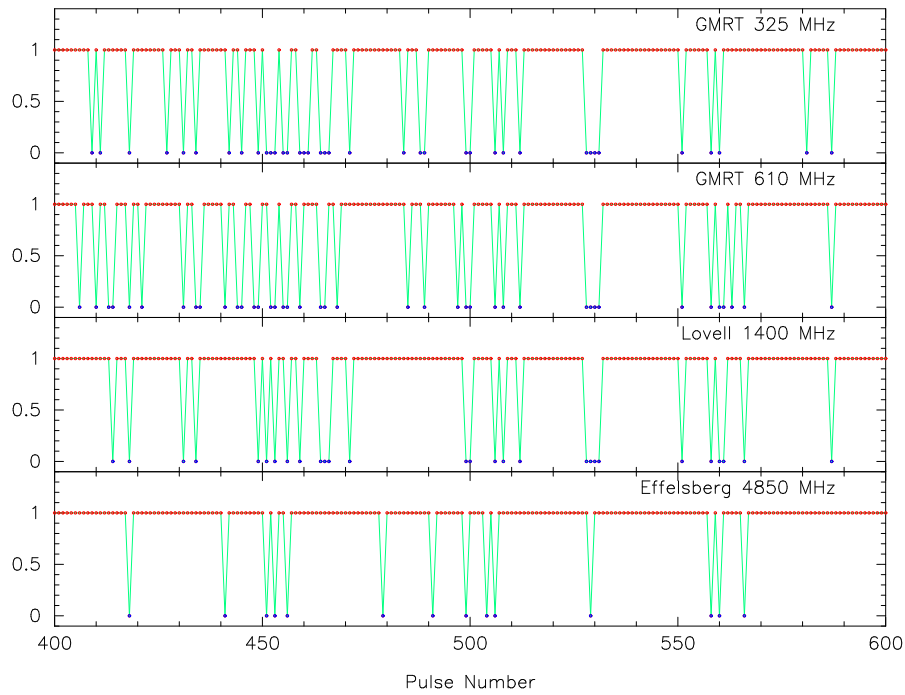


Fig. 3. Binary time series of pulse states at four observing frequencies 325, 610, 1400 and 4850 MHz (top to bottom) for a subset of pulse sequence from the data set II. The time series is generated for a null threshold of $3\sigma_{ep,on}$, where $\sigma_{ep,on}$ is the uncertainty in the pulse energy estimate.

tion², it is the difference between the null count for this combination and that for all four frequencies. For two-frequency combinations, we further exclude selective null pulses for the relevant 3-frequency combinations (e.g., 325+610+1400 MHz and 325+610+4850 MHz for the case of 325+610 MHz). Columns (3) and (5) in Table 2 tabulate such exclusive null counts (and their percentages).

As per Table 2, the most striking case among the various classes of selective nulling is a significantly large number of exclusive null pulses for the frequency combination 325+610+1400 MHz (3.5% and 7.5% respectively for data set I and data set II). The combination 325+610 MHz also shows a significant number of exclusive nulls (2.7% and 1.5% for data set I and data set II respectively). In most other cases (barring the peculiar cases of 610+1400 MHz for data set II, which we address in Appendix A), the number of such exclusive nulls is relatively small ($\lesssim 0.5\%$), and a careful examination of the relevant pulses do not show evidence for any general trend. Therefore, in the bulk of the remainder of this paper, we focus our attention on the most interesting case of simultaneous exclusive nulls at 325+610+1400 MHz. In order to distinguish this special class of nulls from those that are broadband over the full range of observing frequencies, we refer to them as “low frequency nulls” (LF nulls).

5. Selective Nulling: Low Frequency Nulls at 325, 610 and 1400 MHz

We have carefully examined the individual pulses that are grouped as “low frequency nulls,” and find, quite interestingly, that the emission at the highest frequency (4850 MHz) is often

² To denote a specific frequency combination, we insert the “+” symbol in between the relevant frequencies, e.g. the notation “325+610 MHz” refers to the null pulses that are exclusive to 325 and 610 MHz.

marked by a fairly strong, narrow pulse. Examples of this kind of pulses are shown in Fig. 7. In this section, we characterise their properties, and compare and contrast them with those of normal emission seen at this frequency.

5.1. Characterisation of Emission at 4850 MHz

To characterise the high frequency pulses occurring during the LF nulls, we use basic properties such as their width, location and strength. This is done in a two-step process. First, we perform a box car analysis in order to obtain some first order estimates of these quantities. For this, we trial a large number of box car widths (within a range from 0.1 to 0.9 times the main pulse width), deriving the amplitude, location and peak signal-to-noise ratio (S/N) in each case. The case that yields maximum S/N is then taken as the closest representation of the pulse. Using these values as starting points ensures a quick and easy convergence of the finer grid search that is performed subsequently. Here, the amplitude, width and location of the best fit Gaussian is determined using standard chi-square minimisation techniques. These three parameters, along with the peak S/N, are presented in Fig. 8. From this, we can infer the following about the nature of these high frequency emissions:

1. The emission features are often quite strong, with peak S/N typically ~ 50 , while stronger pulses are seen with S/N as large as ~ 300 .
2. Their occurrence is largely confined to a narrow longitude range of $\lesssim 10$ ms, starting roughly $0.25w_p$ from the leading edge of the pulse profile, where w_p is the ON pulse window.
3. There is some evidence for a second preferred location (roughly at $0.75w_p$ from the leading edge), albeit this is mainly seen in data set II.
4. These pulses typically have widths of a few milliseconds, and are usually narrower than the typical subpulses seen during the normal emission.

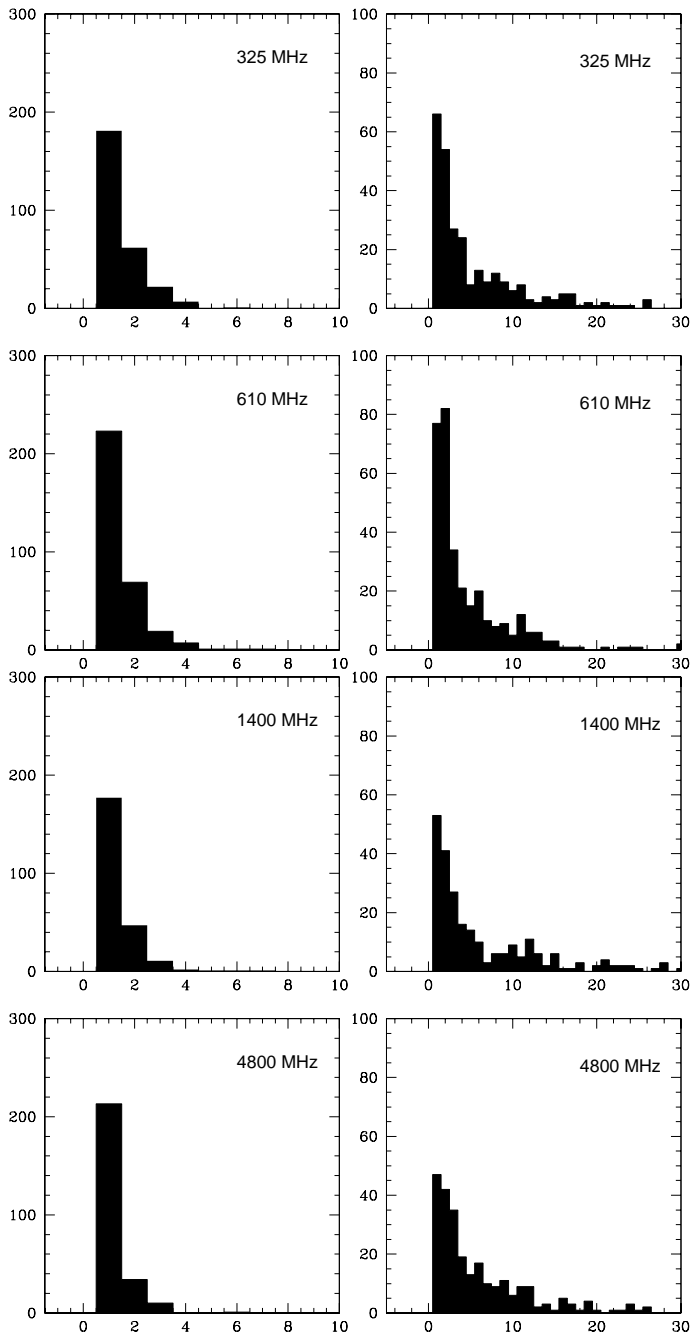


Fig. 5. Histograms of null and burst lengths (left and right panels respectively) constructed from the data set I at the four observing frequencies, 325, 610, 1400 and 4850 MHz. Similar results are also seen for the data set II.

Histograms of the above-mentioned parameters are plotted in Fig. 9 (shaded regions). These are for data set II, however similar trends are also seen for data set I. The S/N and amplitude seem to follow somewhat exponential-like distributions on a linear scale, but we have chosen to plot them on a logarithmic scale in order to better compare and contrast them with the corresponding distributions for the normal population of pulses (see next section). The width distribution is somewhat skewed and is slightly double-peaked in nature. The longitude distributions are nearly symmetric.

5.2. Comparison with “Normal” Emission at 4850 MHz

In order to compare the properties of these high frequency (HF) pulses with those of “normal” pulses, we compute similar parameters for the sample of normal pulses at 4850 MHz. Normal pulses are those which do not belong to either the LF null class or the all-frequency null class. Since this pulsar shows a two-component profile, and given that the high frequency emission during LF nulls tends to occur preferentially in the longitude range of the leading component, we find that it is more appropriate to compare with the properties derived from the leading component only. The results of this exercise are summarised in the histograms shown in Fig. 9 (for data set II), where quantities for the normal population of pulses are shown as unshaded bars. For the reasons described earlier, the S/N and amplitude histograms are plotted on a logarithmic scale. Further, the two distributions are normalised for equal peaks to allow an easy comparison.

From these figures we see that the S/N distribution is narrower and less skewed for the HF emission during LF nulls and it appears to peak at a comparatively higher S/N. The amplitude distributions are also narrower and more symmetric than those for normal pulses. The distributions for widths and locations also show significant differences between the two classes. As inferred qualitatively earlier, the width distribution for the HF pulses is narrower than that for the normal pulses. There is significant spread in the longitudes of occurrence (for both classes), and the spread is more for the normal pulses, thus reinforcing the conclusion that the HF pulses are confined to a narrower range of longitude. Furthermore, the longitude distributions for the LF null class peak at slightly earlier longitudes than those for the normal pulses, indicating that this emission arrives at an earlier phase than that of the normal pulses. Some of these results are clearly seen in a comparison of the average profiles obtained for the two classes of pulses (Fig. 10). These reinforce the conclusions that the HF pulses during LF nulls occur predominantly under the leading component and arrive at an earlier longitude than the normal pulses.

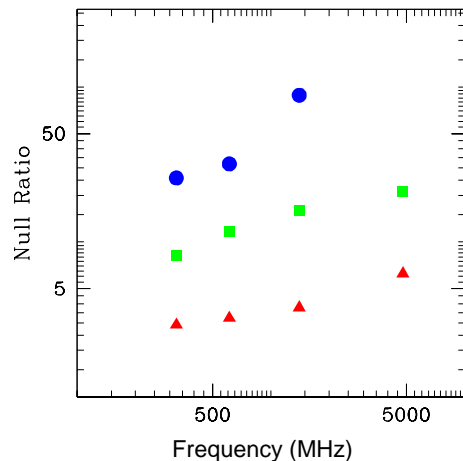


Fig. 6. Plot of “null ratios” as a function of observing frequency. The symbols triangles, squares and circles denote the ratios of the number of single-period nulls to the number of two-period, three-period and four-period nulls, respectively. There is a clear systematic trend with frequency, strongly supporting a frequency dependence of the nulling phenomenon, and suggesting that longer nulls are more common at lower observing frequencies.

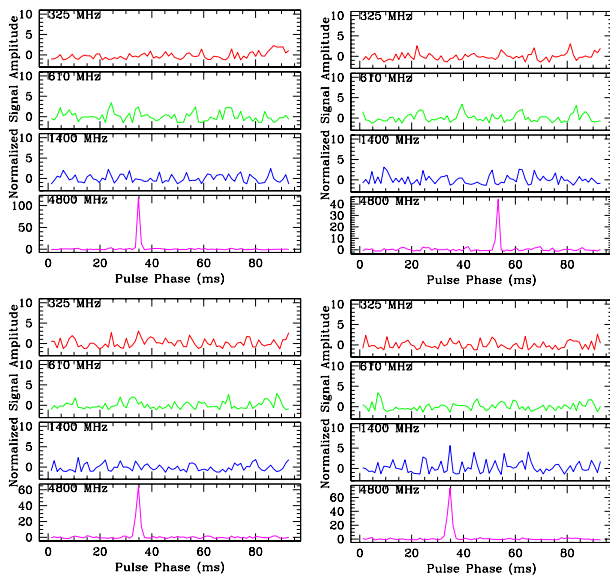


Fig. 7. Examples of low frequency nulls which are marked by a strong, narrow emission feature at the highest frequency of observation, 4850 MHz. These pulses are seen with a signal-to-noise ratio (S/N) as much as 300. The pulse phase window shown in these plots spans approximately 28 degree (92.8 ms) centred at the centre of the integrated pulse profile. The pulse intensities are normalised with off-pulse noise rms after subtracting the mean off-pulse level. No detectable emission seen at the three lower frequencies while the signal is detected with a S/N of 50 to 100 at 4850 MHz.

5.3. Comparison with “Giant Pulses” at 4850 MHz

A different analysis of this data set in Paper IV revealed an interesting sub-class of “giant” pulses for this pulsar at 4850 MHz. These are some of the strongest pulses seen among the non-nulling detections, with typical flux densities more than $10 \times \langle S \rangle$ (where $\langle S \rangle$ is the mean flux density of the entire data), which is the commonly used threshold for detection of giant pulses (e.g. Johnston & Romani (2002)). The emission is often narrow in width and tends to occur preferentially at the *trailing* edge of the leading pulse component (see Fig. 17 of Paper IV). Based on their large flux densities and from the hint of an emerging power-law component in the cumulative distribution of their energies (Fig. 16 of Paper IV), we referred to them as possible giant pulses. However, unlike the classical giant pulses as have been observed for the Crab and a few other pulsars (Cordes et al. 2004; Johnston & Romani 2002), which are characterised by a power-law energy distribution and a spectral index that is comparable to or steeper than that of the normal pulses, these appear to be of a significantly flatter spectrum. This conjecture stems largely from (i) their apparent absence at our lower frequencies and (ii) from observations at a higher frequency of 8450 MHz (Maron & Löhmer, private communication).

It is important to note that in Paper IV we studied the same data set but excluded all pulses with nulls at any frequency in order to compute the spectra. Hence, when studying the nulling pulses and their frequency behaviour as we do in this paper, it is the study of a different subset of pulses. Given this, it is interesting to compare and contrast the population of the aforementioned giant pulses with the HF pulses, as seen during the LF nulls. Both classes are generally strong and narrow, with a mostly single-peaked emission, though the flux densities of the latter are well below the $10 \times \langle S \rangle$ threshold of the former. Further,

they both tend to occur preferentially over some restricted longitude ranges of the leading component: giants near the trailing edge of the leading component (i.e. arriving at a slightly later phase than the normal pulses), and the HF pulses near the leading edge (arriving at a slightly earlier phase than normal pulses). Both show low-number statistics (40 giants and 195 HF pulses) which prevent us from a detailed study of their energy distributions. Their rates of occurrence – typically 1 in 100 for giants and 1 in 20 for HF pulses – are comparable or even larger than the rates of occurrence of giant pulses that are seen for the Crab pulsar (e.g. Cordes et al. 2004). Thus there are some similarities between these two special classes of pulses, and it is possible that they may have related origins.

5.4. Selective Nulling at 325 and 610 MHz

The next most interesting sample in our data set is a subset of pulses that null *exclusively* at 325 and 610 MHz. Some examples are shown in Fig. 11. Although an analysis similar to that described in § 5.1 and § 5.2 was attempted for this class of nulls, the poor statistics of the sample did not allow us to obtain any meaningful characterisation of the emission at higher frequencies for this class of LF nulls. Qualitative examination shows that a majority (~80–90%) of these pulses are characterised by single-peaked emission at 1400 and 4850 MHz, although in most cases the pulse widths do not seem to be significantly narrower than typical sub-pulse widths. As in the case of the first class of HF pulses, the emission here (at 4850 MHz) also tends to occur preferentially at the longitude of the leading component, with only a minority of these pulses appearing at the longitude of the trailing component. Only occasionally, the emission at 1400 and/or 4850 MHz is seen as a double-peaked pulse that is characteristic of the normal emission from this pulsar.

The average profiles (at 1400 and 4850 MHz) of the pulses in this null class are shown in Fig. 12 (green curves), along with

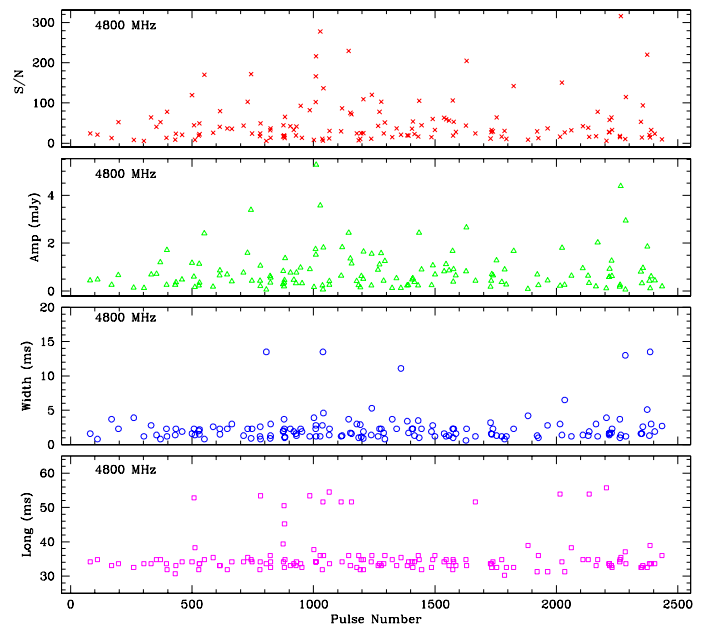


Fig. 8. Properties of the narrow emission features seen at 4850 MHz during the times of low frequency nulls. The quantities plotted here are (from top to bottom) the peak signal-to-noise (S/N), amplitude, width and location (longitude) of these emission features. The results are for the data set II.

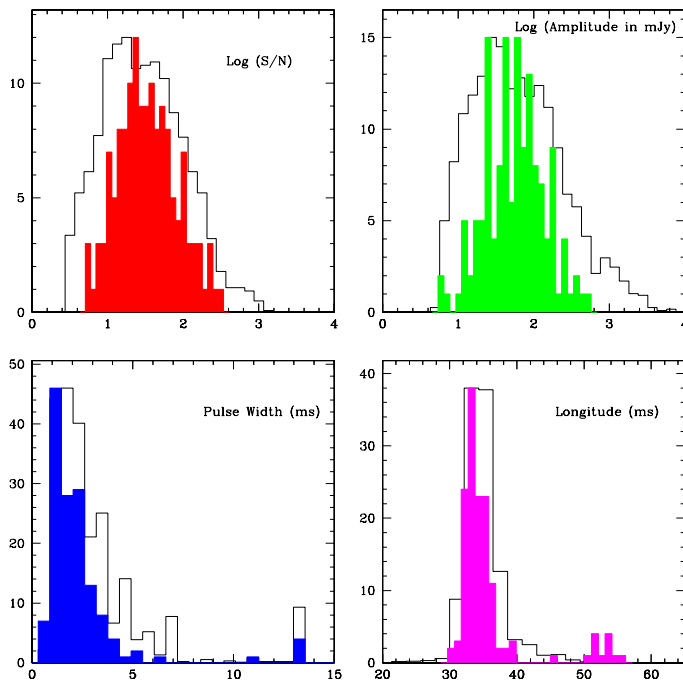


Fig. 9. Properties of the high frequency (4850 MHz) emission during LF nulls (shaded regions) are compared with those of the *normal* emission (for the leading component only) at this frequency. These results are for the data set II. The top panels are the histograms of S/N and amplitude, with data binned at logarithmic intervals. The binning is on a linear scale for the width and longitude distributions (bottom panels).

those of the full sample of normal pulses (red curves). As was the case for the first class of HF pulses, these pulses tend to arrive at a slightly earlier phase than the normal emission, at 4850 MHz. However, no such offset is readily visible for the emission at 1400 MHz.

6. Discussion

In this paper, we focus on the analysis of the pulse nulling phenomenon in PSR B1133+16 using high-quality single-pulse data from simultaneous multifrequency observations. The most important finding from our analysis is that nulling *does not always occur simultaneously* at all frequencies. Our observations un-

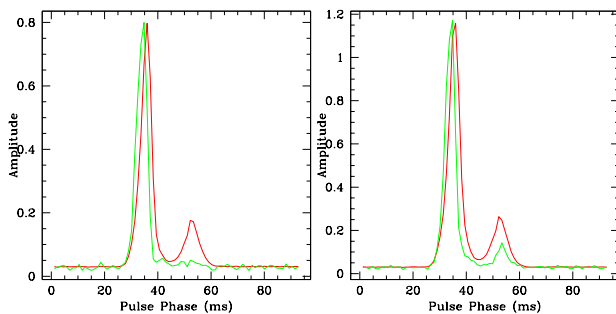


Fig. 10. Average profiles of the emission at 4850 MHz during the low frequency nulls (green curves) overlaid on those of the normal pulses (red curves); *left*: the data set I, and *right*: the data set II. The peaks of the two profiles are slightly offset, indicating a tendency for the pulses during low frequency nulls to arrive at a slightly earlier phase.

cover a significant number of pulses ($\approx 6\%$) that null at the three lower frequencies of our observation, however are marked by quite narrow and strong pulses at the highest frequency of 4850 MHz. Their properties seem to be quite different from those of the normal pulses seen at this frequency, but interestingly, show some striking similarities with the subset of the strongest pulses in such a sample. Our analysis shows some evidence for the number of simultaneous null pulses to decrease with the frequency coverage of the data, and also suggests that longer-duration nulls are relatively more common at the lower observing frequencies. In the remainder of the paper, we review what has been learnt so far about the nulling behaviour of this pulsar from past observations and discuss possible implications for pulsar emission.

6.1. Comparison with Previous Nulling Studies

PSR B1133+16 is among the well-studied pulsars since the early days of pulsar observations (Backer 1972; Boriakoff 1983; Ferguson & Seiradakis 1978; Kardashev et al. 1982; Smirnova et al. 1994). Its nulling behaviour is not extreme as in the case of PSR B0031-07 and PSR B1944+17 (Deich et al. 1986; Huguenin et al. 1970), which are known for their long durations of nulling (null fractions of the order $\sim 50\%$). In fact, most null durations of this pulsar are within the range of one to a few pulse periods, with a moderately large null fraction (~ 10 to 20%) over typical observing durations. It is also important to recognise that most nulling studies to date have been based on data taken at a single observing frequency. Interestingly, our estimates of null fraction at single frequencies (with the exception of 4850 MHz for data set II and barring the special cases of 610 and 1400 MHz for data set II; see Appendix A), are comparable to the published estimate of $15 \pm 3\%$ from earlier studies (Biggs 1992; Ritchings 1976). However, the null fraction of real “broadband” nulls (i.e., nulls that simultaneously occur at all four frequencies of observation) is only $\approx 7.5\%$. Thus, in general, most published estimates for null fraction are likely to be overestimates if broadbandness is adopted as an additional criterion to define a truly null state.

There have been several single-pulse studies of PSR B1133+16 in the past based on data from simultaneous observations at multiple frequencies (Backer & Fisher 1974; Bartel & Sieber 1978; Boriakoff 1983; Boriakoff & Ferguson 1981; Kardashev et al. 1982), and it is fairly well established that the pulse energy and structure of this pulsar are well correlated at single-pulse, sub-pulse and micro-pulse levels. Specifically, the works of Boriakoff (1983) and Kardashev et al. (1982) addressed the broadbandness of micropulse and subpulse structure, while Bartel & Sieber (1978) focussed on the microstructure of single pulses in this pulsar. However, none of these studies were able to address the simultaneity in pulse nulling at different observing frequencies. In fact, there have been few studies that have even peripherally addressed this interesting phenomenon. The only relevant work that we are aware of in this context is by Davies et al. (1984) who studied simultaneous data of PSR B0809+74 taken at 102 and 406 MHz. In their short stretch of data (348 pulse periods), they recorded 9 nulls at 102 MHz, and only 3 at 406 MHz. Interestingly nulls at 406 MHz always correspond to nulls at 102 MHz, but not vice versa. While this may not qualify as a strong supporting evidence for selective nulling, it does suggest that the pulsar nulling characteristics vary with observing frequency.

6.2. Implications for Pulsar Emission Models

In sections §5.1 and §5.2, we compared and contrasted the characteristics of the high frequency emission during low frequency nulls with the “normal” emission at 4850 MHz. We also compared them with those of “giant” pulses as reported in our earlier paper (§5.3). Based on our analysis, we would like to conjecture that (a) the high frequency emission pulses are different from the normal pulses and are likely to be related to the “giant” pulses; (b) the spectrum of these “giants” is probably flatter, and consequently they are more easily seen at higher frequencies (Paper IV); and (c) we see them when the normal radio emission is off or too weak to be detectable (i.e. nulling) at high frequencies (this paper).

One of the most interesting results from our analysis is the observation of narrow high frequency pulses at times of low frequency nulls. The simplest possible interpretation could be the presence of an *additional* process of emission that does *not* turn off when the pulsar switches to a “null state” at low frequencies. It is also quite possible that such a process is more like a gradual effect, becoming predominant above a cutoff frequency. Unfortunately, our data are insufficient to address such a hypothesis.

Our data also show several instances of significant emission at both 1400 and 4850 MHz, when there occurs a null at the lower frequencies. However, the results are not conclusive enough to suggest a frequency dependence for such an additional process. A likely scenario is that the emission tends to be narrower and peaks at an earlier phase with an increase in frequency.

It is possible that such an additional emission process is also present during the normal emission. However, given that the pulsar’s emission is typically double-peaked and has a strong lead-

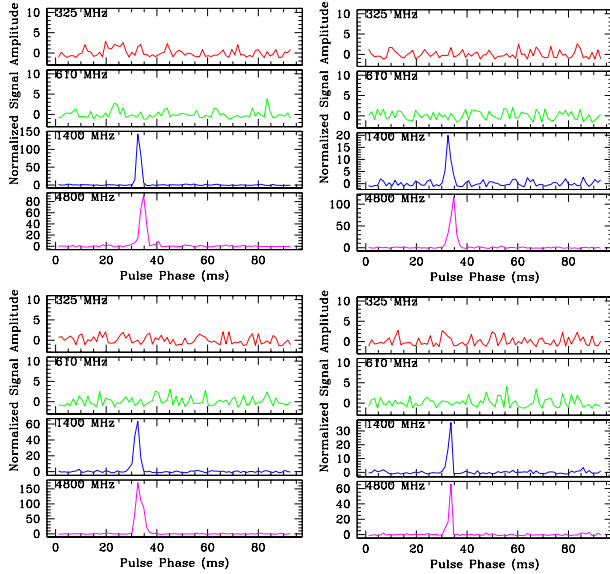


Fig. 11. Examples of pulses that null at the lower two observing frequencies, 325 and 610 MHz, while the emission is seen – mostly as narrow, single-peaked pulses – at the two higher frequencies, 1400 and 4850 MHz. Statistics of this class of pulses is however not good enough to construct meaningful histograms such as in Fig. 9 (see text). The pulse intensities are normalised in a manner similar to that in Fig. 7. No detectable emission is seen at 325 and 610 MHz even upon averaging all the null pulses at these frequencies.

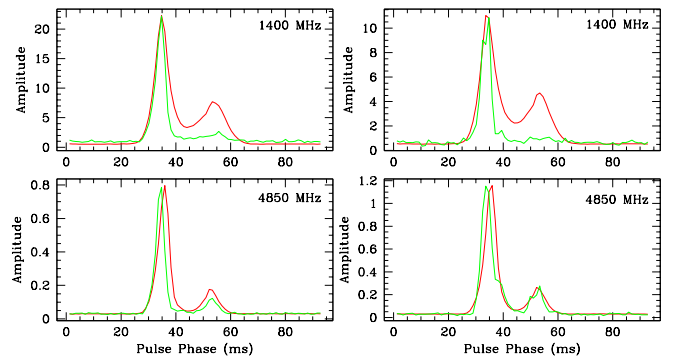


Fig. 12. Average profiles constructed from the subsets of pulses where the emission is seen at 1400 and 4850 MHz, while the pulsar switches to a “null state” at 325 and 610 MHz (green curves). Overlaid are the average profiles constructed from the sample of normal pulses at these frequencies (red curves). The emission at both frequencies tends to occur preferentially at the longitude of the leading pulse component; the profiles are nearly peak-aligned at 1400 MHz (top panels), while a slight phase offset is evident for those at 4850 MHz (bottom panels). The profiles of the subsets are scaled for a close match with the peaks of the average profiles of the normal pulses. The left and right panels correspond to the data sets I and II respectively.

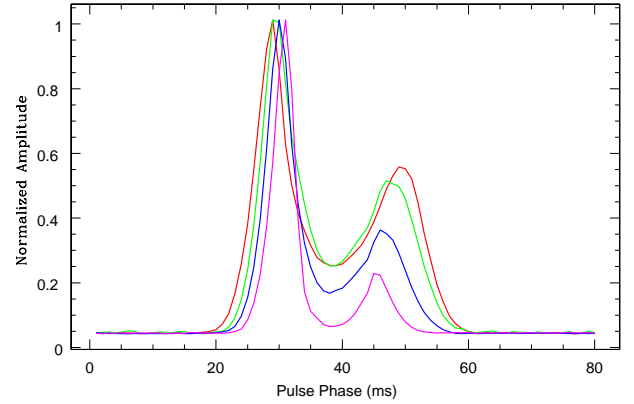


Fig. 13. Integrated pulse profiles at all four frequencies of observation; 325 MHz (red), 610 MHz (green), 1400 MHz (blue), and 4850 MHz (magenta). These profiles are constructed from data that are already time-aligned and corrected for frequency-dependent dispersive delays. Further, they are normalised for equal peaks of the leading pulse components. The relative strength of the leading pulse component shows a systematic increase with an increase in frequency.

ing pulse component, its presence might be hard to discern in non-nulling pulses. Assuming this may be the case, we would expect a significant increase in relative strength of leading and trailing pulse components with an increase in frequency, which is indeed seen for this pulsar (Fig. 13).

An alternate, and perhaps more likely, possibility involves this emission being related to the population of “giant” pulses (as discussed in § 5.3). In particular, given their preferred longitudes of occurrence near the leading pulse component, a likely flat-spectrum nature, and above all, a tendency to occur even when the pulsar nulls at low frequencies, may also suggest that they probably originate in a different part of the magnetosphere which does not participate in nulling. If this is the case, it may support an outer gap origin as opposed to a polar cap region (where

nulling is probably more effective). Such a scenario might also suggest a possible link to some high-energy emission processes that occur in the outer parts of the magnetosphere. Future simultaneous observations of this pulsar, preferably with a denser sampling of frequency in the $\sim 1\text{--}5$ GHz range, should enable us to address this in more detail.

7. Conclusions

We have studied high-quality single-pulse data of PSR B1133+16 from simultaneous multifrequency observations conducted using the GMRT, Lovell and Effelsberg to perform an in-depth analysis of the pulse nulling phenomenon. Our observations provided long data stretches over a wide frequency range (from 0.3 to 4.85 GHz), which allow, for the first time, investigation of nulling as a function of observing frequency, separation in frequency as well as combination of frequencies. The data shows that the pulsar spends approximately 15% of the time in a null state at our frequencies of observation. However, only roughly half of these nulls occur simultaneously at all four frequencies. In other words, much in contrary to the traditional notion of being a broadband phenomenon, nulling does *not always* occur simultaneously at all four frequencies.

Our most interesting finding of this “selective nulling” phenomenon is a significantly large number of pulses ($\approx 5\%$) that show an emission at the highest frequency of our observation, 4850 MHz, while there occurs a null at all three lower frequencies (325, 610 and 1400 MHz). This emission is often seen as fairly strong and narrow pulses, and is different from the broad, double-peaked emission normally seen from this pulsar. We have characterised these high frequency pulses in terms of their amplitudes, widths and locations, and compared their statistical properties with those of the leading component of the normal pulses. Our analysis reveals significant differences in the properties between the two classes. Specifically, the population of HF pulses shows an amplitude distribution that is more skewed, a comparatively narrower width distribution, and a tendency to arrive at a slightly earlier phase than the leading pulse component. Additionally, we note some interesting similarities between these narrow pulses and the “giant” pulses as identified for this pulsar in our earlier paper.

We do not have any clear and convincing explanation to offer at this point, apart from the simplest (and rather speculative) interpretation involving the presence of an additional emission process that does not turn off even when the pulsar nulls at lower frequencies. Alternatively, such an additional process may be a gradual effect that becomes more predominant at higher frequencies. While our data are insufficient to address such hypotheses, such scenarios could potentially result in observable effects such as an increase in relative strength between the leading and trailing pulse components at higher observing frequencies, which is indeed seen for this pulsar.

Given the significant similarities between this emission and “giant” pulses as seen at 4850 MHz, it is quite possible that they share a common, or at least related, origin. In particular, their tendency to occur at specific pulse longitudes, along with the pulse shapes and spectral characteristics that are different from the normal emission, add support to such a conjecture and are suggestive of a likely origin in the outer parts of the magnetosphere. We hope future simultaneous observations will help to shed more light on such possibilities.

Acknowledgements: We are grateful to all the people working at the participating telescopes who made these observations possi-

ble. In particular we thank S. Kudale, M. Jangam and C. Lange for assistance with the observations, and R. Wielebinski for the encouragement and support towards this project. We also thank an anonymous referee for a critical review and several insightful comments which helped improve the contents and presentation of the paper. The Giant Metrewave Radio Telescope (GMRT) is operated by the National Centre for Radio Astrophysics of Tata Institute of Fundamental Research.

References

- Backer, D. C. 1970, *Nature*, 228, 42
- Backer, D. C. 1972, *ApJ*, 174, L157
- Backer, D. C. & Fisher, J. R. 1974, *ApJ*, 189, 137
- Bartel, N. & Sieber, W. 1978, *A&A*, 70, 307
- Bhat, N. D. R., Rao, A. P., & Gupta, Y. 1999, *ApJS*, 121, 483
- Bhat, N. D. R., Karastergiou, A., Gupta, Y., Kramer, M., & Lyne, A. G. 2001, *BAAS*, 34, 569
- Biggs, J. D. 1992, *ApJ*, 394, 574
- Boriakoff, V. 1983, *ApJ*, 272, 687
- Boriakoff, V. & Ferguson, D. C. 1981, *IAU Symp.* 95: Pulsars: 13 Years of Research on Neutron Stars, 95, 191
- Cordes, J. M., Bhat, N. D. R., Hankins, T. H., McLaughlin, M. A., & Kern, J. 2004, *ApJ*, 612, 375
- Cordes, J. M., Pidwerbetsky, A., & Lovelace, R. V. E. 1986, *ApJ*, 310, 737
- Davies, J. G., Lyne, A. G., Smith, F. G., Izvekova, V. A., Kuzmin, A. D., & Shitov, I. P. 1984, *MNRAS*, 211, 57
- Deich, W. T. S., Cordes, J. M., Hankins, T. H., & Rankin, J. M. 1986, *ApJ*, 300, 540
- Durbin, J. M., Large, M. I., Little, A. G., Manchester, R. N., Lyne, A. G., & Taylor, J. H. 1979, *MNRAS*, 186, 39
- Ferguson, D. C., & Seiradakis, J. H. 1978, *A&A*, 64, 27
- Gupta, Y., Gothoskar, P., & Bhat, N. D. R. 2002, *IAU Symposium*, 199, 369
- Huguenin, G. R., Taylor, J. H., & Troland, T. H. 1970, *ApJ*, 162, 727
- Johnston, S. & Romani, R. W. 2002, *MNRAS*, 332, 109
- Karastergiou, A., von Hoensbroech, A., Kramer, M., Lorimer, D. R., Lyne, A. G., Doroshenko, O., Jessner, A., Jordan, C. & Wielebinski, R. 2001, *A&A*, 379, 270
- Karastergiou, A., Kramer, M., Johnston, S., Lyne, A. G., Bhat, N. D. R., & Gupta, Y. 2002, *A&A*, 391, 247
- Karastergiou, A., Johnston, S., & Kramer, M. 2003, *A&A*, 404, 325
- Kardashev, N. S., Nikolaev, N. I., Novikov, A. I., Popov, M. V., Soglasnov, V. A., Kuzmin, A. D., Smirnova, T. V., Bartel, N., Sieber, W. & Wielebinski, R. 1982, *A&A*, 109, 340
- Kramer, M., Karastergiou, A., Gupta, Y., Johnston, S., Bhat, N. D. R., & Lyne, A. G. 2003, *A&A*, 407, 655
- Lorimer, D. R., Jessner, A., Seiradakis, J. H., Lyne, A. G., D’Amico, N., Athanasopoulos, A., Xilouris, K. M., Kramer, M. & Wielebinski, R. 1998, *A&AS*, 128, 541
- Rankin, J. M. 1986, *ApJ*, 301, 901
- Rickett, B. J. 1990, *ARA&A*, 28, 561
- Ritchings, R. T. 1976, *MNRAS*, 176, 249
- Robinson, B. J., Cooper, B. F. C., Gardner, F. F., et al. 1968, *Nature*, 218, 1143
- Romani, R. W., Narayan, R., & Blandford, R. 1986, *MNRAS*, 220, 19
- Smirnova, T. V., Tul’bashev, S. A., & Boriakoff, V. 1994, *A&A*, 286, 807

Appendix A: Scintillation Fading and Nulling Statistics

Here we address the peculiar case of a large number of nulls seen at 610 and 1400 MHz for data set II. On a careful examination, we find that a majority of these nulls are largely clustered into two groups, the first in the range ~ 1200 to ~ 1500 in pulse number, and the second in the range ~ 2200 to ~ 2500 . Interestingly, these regions of occurrence correlate well with the regions of flux fading seen at these frequencies. We therefore propose that the apparent excess in null counts and simultaneous nulls exclusive to these frequencies is essentially a manifestation of scintillation-induced flux fading. Below we elaborate on our arguments.

As is well known, pulsar signals are subject to interstellar scintillation (ISS), observable effects of which are strongly frequency dependent. At low observing frequencies, most pulsars are in the strong scintillation regime, where the observable effects can be grouped into two distinct classes, viz., diffractive and refractive scintillation (e.g. Cordes, Pidwerbetsky, & Lovelace 1986; Rickett 1990; Romani, Narayan, & Blandford 1986), with consequences such as flux density variations exhibiting two characteristic time scales. At frequencies higher than a few GHz, most nearby pulsars transition to the weak scintillation regime, which is marked by a single characteristic time scale (Rickett 1990). PSR B1133+16 is expected to be in the strong scattering regime at 325, 610 and 1400 MHz, and in weak scintillation at our highest observing frequency of 4850 MHz (see Paper IV for details on relevant scintillation parameters).

For observations at low observing frequencies ($\lesssim 1$ GHz), the dominant ISS effect is random intensity modulations due to diffractive scintillation (e.g. Bhat, Rao, & Gupta 1999). The pulse intensity decorrelates over narrow ranges in time and frequency, and the decorrelation widths ($\Delta\nu_{iss}$ and Δt_{iss} respectively in frequency and time) are strongly frequency dependent ($\Delta\nu_{iss} \sim \nu^{4.4}$, $\Delta t_{iss} \sim \nu^{1.2}$, where ν is the frequency of observation). Thus, intensity modulations as deep as 100% can be expected over time and frequency scales of Δt_{iss} and $\Delta\nu_{iss}$. For observations made over time durations (t_{obs}) much larger than Δt_{iss} , three regimes may be identified for apparent intensity modulations, depending on the ratio of the scintillation bandwidth ($\Delta\nu_{iss}$) to the total bandwidth of observation, ΔB : (i) $\Delta B \gg \Delta\nu_{iss}$: here the effective flux modulations will be quenched to some extent depending on the ratio $\Delta B / \Delta\nu_{iss}$; (ii) $\Delta B \sim \Delta\nu_{iss}$, i.e. when the observing bandwidth is comparable to the scintillation bandwidth: flux fading as large as $\sim 100\%$ is likely to occur over durations of Δt_{iss} ; (iii) $\Delta B \ll \Delta\nu_{iss}$, such deep flux fading could still occur over Δt_{iss} , albeit with somewhat less likelihood.

Consider the scenario where simultaneous observations made at three different frequencies correspond to the three different cases described above. There could be rare instances of simultaneous flux fading at the two frequencies that correspond to cases (ii) and (iii). Such apparent nulls may lead to consequences such as an increase in null counts as well as an increase in the number of simultaneous nulls exclusive to those frequencies. A comparison of the scintillation and observing parameters for PSR B1133+16 at 610 and 1400 MHz ($\Delta\nu_{iss} \sim 11$ MHz, $\Delta t_{iss} \sim 6$ min at 610 MHz; $\Delta\nu_{iss} \sim 270$ MHz, $\Delta t_{iss} \sim 16$ min at 1400 MHz) supports such a conjecture.

Some simple checks could help reaffirm this. Since Δt_{iss} increases with the observing frequency, we would expect the time span of such apparent nulls to be limited to Δt_{iss} at the lower frequency, i.e. 610 MHz. Interestingly, the observed duration of 300 pulses (≈ 6 min) is in excellent agreement with the expected value for Δt_{iss} at 610 MHz. Further, Δt_{iss} at 1400 MHz is expected to be roughly 3 times larger than that at 610 MHz. This means we can expect null counts at these two frequencies to increase by roughly 4% and 12% in comparison to the measured values for the data set I. Though the observed excess is somewhat larger than this, it does conform to the expectation that larger excess should be seen at 1400 MHz. In short, the increase in null counts and a larger number of exclusive nulls at 610 and 1400 MHz for data set II can be attributed to the combination of ISS and our observing parameters.